Composite Schemes on Triangular Meshes

Karel Kozel, Michal Janda and Richard Liska

Abstract. The composite schemes are given by the global composition of several steps of Lax-Wendroff scheme followed by one step of Lax-Friendrichs scheme bringing sufficient diffusion to smooth out dispersive Lax-Wendroff oscilations. The composite schemes are generalized to triangular mesh by finite volume approach. Several numerical results for transonic flows through a channel are presented in 2D and also in 3D extension.

1. Introduction

The basic idea of the composite schemes [1] in 1D is very simple. It is well-known that the Lax-Wendroff (LW) scheme is oscillating behind the shocks while the Lax-Friedrichs (LF) scheme is excessively diffusive. The composite schemes use after several LW steps one LF step as a consistent filter removing the LW oscillations. This simple idea works remarkably well not only in 1D but also in higher dimensions. The new 2D finite volume schemes of LF and LW type on a rectangular mesh together with their composition have been presented in [1]. Their extensions to a trapezoidal mesh [2] and to general logically rectangular meshes consisting of general quadrilaterals [3] have proved to work also well. The direct generalization of the 2D LW scheme to 3D on rectangular grid was unstable however it is possible to stabilize it [4] and it also produces nice results. As these schemes use neither Riemann solvers, nor eigenvector decomposition they are fast and being explicit ones they are ideally suited to vectorization and/or parallelization.

Here we present generalization of these composite schemes to a triangular mesh in the finite volume form of cell-centered and cell-vertex schemes. Basic mesh is a triangular mesh and all methods can also be formulated on an unstructured triangular mesh or even on combined triangular-quadrilateral mesh when Euler equations are considered.

Authors present numerical results of 2D transonic flows through a GAMM channel (steady and unsteady) and also through channel changed by two bumps (cascade geometry). The method was extended to 3D case and also some 3D results in a channel are presented.

2. Finite volume schemes

We consider Euler equations which in the most general 3D case written in a conservative form are

$$W_t + F_x + G_y + H_z = 0, \qquad (1)$$
$$W = (\rho,\, \rho u,\, \rho v,\, \rho w,\, e)^T,$$

where ρ is density, $(u, v, w)^T$ velocity vector, e total energy per unit volume.

In the simplest 1D case there are two forms of Lax-Friedrichs(LF) scheme $(\sigma = \frac{\Delta t}{\Delta x})$:

1. standard one-step version – non-staggered

$$\begin{aligned} W_i^{n+1} &= \frac{1}{2}\left(W_{i+1}^n + W_{i-1}^n\right) - \frac{\sigma}{2}\left(F_{i+1}^n - F_{i-1}^n\right) = \\ &= W_i^n - \frac{\sigma}{2}\left(F_{i+1}^n - F_{i-1}^n\right) + \frac{1}{2}\left(W_{i+1}^n - 2W_i^n + W_{i-1}^n\right) \end{aligned} \qquad (2)$$

$$\text{or instead} \quad \frac{1}{2}\left(W_{i+1} - 2W_i + W_{i-1}\right) \to \frac{\varepsilon}{2}\left(W_{i+1}^n - 2W_i^n + W_{i-1}^n\right),\ \varepsilon \in (0, 1\rangle. \qquad (3)$$

2. two-step version with staggered grid

$$\begin{aligned} W_{i+\frac{1}{2}}^* &= \frac{1}{2}\left(W_{i+1}^n + W_i^n\right) - \frac{\sigma}{2}\left(F_{i+1}^n - F_i^n\right) \\ W_i^{n+1} &= \frac{1}{2}\left(W_{i+\frac{1}{2}}^* + W_{i-\frac{1}{2}}^*\right) - \frac{\sigma}{2}\left(F_{i+\frac{1}{2}}^* - F_{i-\frac{1}{2}}^*\right) \end{aligned} \qquad (4)$$

$$\text{or only} \quad W_i^{n+\frac{1}{2}} = \frac{1}{2}\left(W_{i+\frac{1}{2}}^* + W_{i-\frac{1}{2}}^*\right). \qquad (5)$$

One can observe that (5) is (3) with $\varepsilon = \frac{1}{2}$. One-step form of (4) is

$$\begin{aligned} W_i^{n+1} &= W_i^n - \frac{\sigma}{2}\left(F_{i+1}^n - F_{i-1}^n\right) + \frac{1}{4}\left(W_{i+1}^n - 2W_i^n + W_{i-1}^n\right) + \\ &+ \frac{1}{4}\left(\sigma A^n\right)^2\left(W_{i+1}^n - 2W_i^n + W_{i-1}^n\right) \end{aligned} \qquad (6)$$

where quasi-conservation form is used $\left(A = \frac{\partial F}{\partial W}\right)$.

In analogy with (2) and (4) two two-step version s of the Lax-Wendroff (LW) scheme can be written down as:

1. non-staggered

$$\begin{aligned} W_i^{n+\frac{1}{2}} &= W_i^n - \frac{\sigma}{4}\left(F_{i+1}^n - F_{i-1}^n\right) + \frac{\varepsilon}{2}\left(W_{i+1}^n - 2W_i^n + W_{i-1}^n\right),\ \varepsilon \in (0, 1\rangle, \\ W_i^{n+1} &= W_i^n - \frac{\sigma}{2}\left(F_{i+1}^{n+\frac{1}{2}} - F_{i-1}^{n+\frac{1}{2}}\right) \end{aligned} \qquad (7)$$

2. staggered

$$
\begin{aligned}
W_{i+\frac{1}{2}}^{n+\frac{1}{2}} &= \frac{1}{2}\left(W_{i+1}^{n} + W_{i}^{n}\right) - \frac{\sigma}{2}\left(F_{i+1}^{n} - F_{i}^{n}\right), \\
W_{i}^{n+1} &= W_{i}^{n} - \sigma\left(F_{i+\frac{1}{2}}^{n+\frac{1}{2}} - F_{i-\frac{1}{2}}^{n+\frac{1}{2}}\right). \qquad (8)
\end{aligned}
$$

A composite scheme LWLFN is given by $(N-1)$ LW steps followed by one LF step $C(U) = LF(LW^{N-1}(U))$ [1].

A general finite volume scheme in 2D is given by

$$
W_{i}^{n+1} = W_{i}^{n} - \frac{\Delta t}{\mu_i}\iint\limits_{D_i} F dy - G dx \doteq W_{i}^{n} - \frac{\Delta t}{\mu_i}\sum_{k=1}^{m} \tilde{F}_k \Delta y_k - \tilde{G}_k \Delta x_k, \quad (9)
$$

$$
\mu_i = \iint\limits_{D_i} dx dy,
$$

where $\tilde{F}, \tilde{G}$ are numerical fluxes approximating physical fluxes F, G. Now we can extend both versions of 1D schemes to 2D or 3D finite volume ones. Consider e.g. triangular mesh with finite volumes T_i. Then the cell-centered scheme corresponding to the non-staggered 1D version will be

LF:

$$
W_{i}^{n+\frac{1}{2}} = \frac{1}{3}\sum_{k=1}^{3} W_{k}^{n} - \frac{1}{2}\frac{\Delta t}{\mu_i}\sum_{k=1}^{3}\left(F_{k,i}^{n}\Delta y_k - G_{k,i}^{n}\Delta x_k\right) \quad (10)
$$

or $$W_{i}^{n+\frac{1}{2}} = W_{i}^{n} - \frac{1}{2}\frac{\Delta t}{\mu_i}\sum_{k=1}^{3}\left(F_{k,i}^{n}\Delta y_k - G_{k,i}^{n}\Delta x_k\right) + \frac{\varepsilon}{3}\sum_{k=1}^{3}\left(W_{k}^{n} - W_{i}^{n}\right) \quad (11)$$

where $\mu_i = \iint\limits_{T_i} dx dy$, $F_{k,i}^{n} = \frac{1}{2}(F_k^n + F_i^n)$, $G_{k,i}^{n} = \frac{1}{2}(G_k^n + G_i^n)$, $\varepsilon \in (0, 1\rangle$ and W_k is the value of W at one of three neighboring triangles T_k $(k = 1, 2, 3)$ of the triangle T_i (see Fig. 1).

LW:

$$
W_{i}^{n+\frac{1}{2}} \quad \text{is given by LF (10)} \quad (12)
$$

$$
W_{i}^{n+1} = W_{i}^{n} - \frac{\Delta t}{\mu_i}\sum_{k=1}^{3}\left(F_{k,i}^{n+\frac{1}{2}}\Delta y_k - G_{k,i}^{n+\frac{1}{2}}\Delta x_k\right) \quad (13)
$$

The cell-vertex scheme corresponding to the 1D staggered version has the following form (assuming that six triangles meet at each vertex)

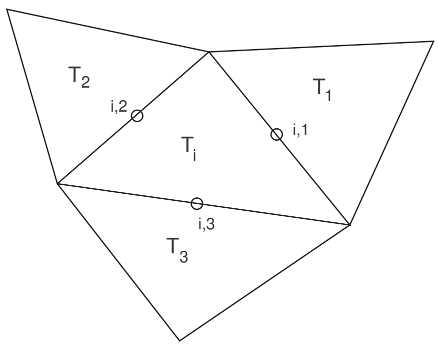

FIGURE 1. Triangles used in the 2D cell-centered scheme.

LF:

$$W_i^* = \frac{1}{3}\sum_{k=1}^{3} W_{0k}^n - \frac{\Delta t}{2\mu_i}\sum_{k=1}^{3}\left(\tilde{F}_k^n \Delta y_k - \tilde{G}_k^n \Delta x_k\right) \tag{14}$$

$$\tilde{F}_k = \frac{1}{2}\left[F_{0,k+1} - F_{0,k}\right],\ \tilde{G}_k = \frac{1}{2}\left[G_{0,k+1} - G_{0,k}\right]$$

$$W_{0,k}^{n+1} = \frac{1}{6}\sum_{i=1}^{6} W_{0,i}^* - \frac{\Delta t}{2\mu_{0k}}\sum_{i=1}^{6}\left(\tilde{F}_i^* \Delta y_i - \tilde{G}_i^* \Delta x_i\right) \tag{15}$$

$$\tilde{F}_i^* = \frac{1}{2}\left[F_{i+1}^* - F_i^*\right],\ \tilde{G}_i^* = \frac{1}{2}\left[G_{i+1}^* - G_i^*\right]$$

LW has the predictor of LF scheme (14) and the corrector

$$W_{0,k}^{n+1} = W_{0,k}^n - \frac{\Delta t}{\mu_{0k}}\sum_{i=1}^{6}\left(\tilde{F}_i^* \Delta y_i - \tilde{G}_i^* \Delta x_i\right). \tag{16}$$

Here $W_{0,k}$ are located at vertices $V_{0,i}$ of triangle T_i, W_i^* are located at the centers of gravity P_i of triangles T_i, $W_i^* = W^*(P_i)$ and $F_i^* = F(W_i^*)$, $G_i^* = G(W_i^*)$ (see Fig. 2).

The stability of the cell-vertex schemes has been investigated by numerical sampling of amplification factor for the scalar advection equation $u_t + au_x + bu_y = 0$ on uniform grid of equilateral triangles with edge length Δx. The LF scheme (14), (15) is stable for $\lambda^2 + \mu^2 \le 2/3$ ($\lambda = a\Delta t/\Delta x, \mu = b\Delta t/\Delta x$). The stability constrain of the LW scheme (14), (16) is little bit less restrictive.

In cell-centered form one performs two steps in LF and predictor-corrector steps in LW, while in cell-vertex form one performs predictor-corrector steps in both LF and LW schemes. The composite scheme LWLFN is defined as in 1D. Suitable number N has to be chosen by testing.

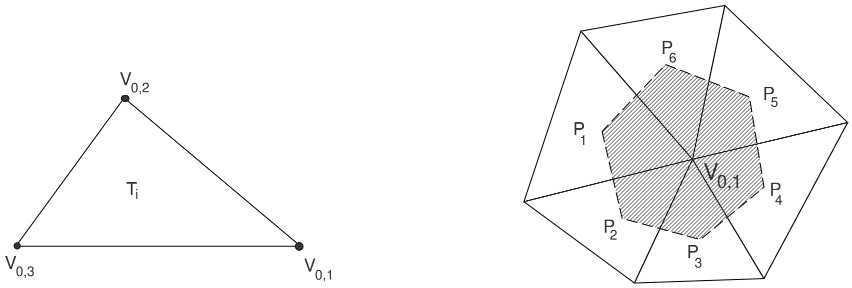

(a) (b)

FIGURE 2. Volumes of 2D cell-vertex scheme: (a) basic volume (grid of triangles); (b) dual volume associated with the point $V_{0,1}$

Cell-vertex form of our scheme has been extended to 3D problems. We expected extension of 2D GAMM channel with a bump varying in the third direction. For such configuration (see the real grid at Fig. 7) we use a grid which is triangular in 2D and layered in the third direction, so that basic volumes are heptahedra (see Fig. 3a). Construction of dual volumes is shown in Fig. 3b.

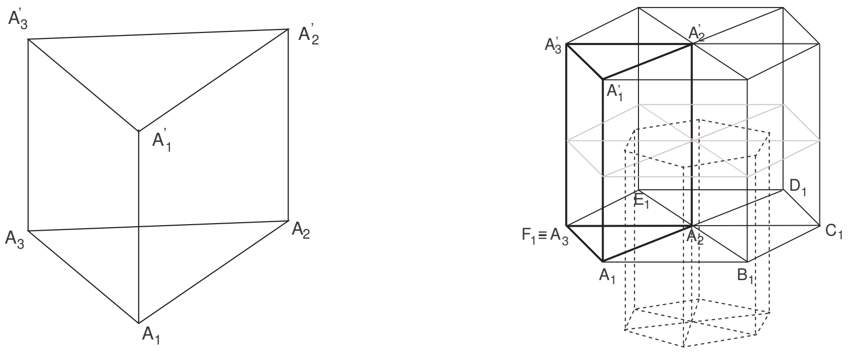

(a) (b)

FIGURE 3. Volumes of 3D cell-vertex scheme: (a) basic volume – heptahedron (b) dual volume associated with the point $A_{0,1}$

The LF and LW finite volume cell-vertex schemes for our grid are:

LF:

$$W_i^* = \frac{1}{6}\sum_{k=1}^{6} W_{0,k}^n - \frac{1}{2}\frac{\Delta t}{\mu_0}\sum_{k=1}^{5}(F,\, G,\, H)_{0,k}^n \cdot \overrightarrow{\Delta S_k} \tag{17}$$

$$W_{0,i}^{n+1} = \frac{1}{12}\sum_{i=1}^{12} W_i^* - \frac{1}{2}\frac{\Delta t}{\mu_{0,i}}\sum_{i=1}^{8}(F,\,G,\,H)_i^* \cdot \overrightarrow{\Delta S_i} \tag{18}$$

Predictor step is realized using finite volume shown in Fig. 3a and for corrector in Fig. 3b.

LW:

Predictor step is (17) and corrector computed by (19)

$$W_{0,i}^{n+1} = W_{0,i}^{n} - \frac{\Delta t}{\mu_{0,i}}\sum_{i=1}^{8}(F,\,G,\,H)_i^* \cdot \overrightarrow{\Delta S_i} \tag{20}$$

3. Some numerical results

We have tested both schemes for steady subsonic and transonic flows in the GAMM channel (parallel walls with a 10% bump at the lower wall) with $M_\infty = 0.5$ (subsonic flow) and $M_\infty = 0.675$. The structure of inviscid flow, especially for transonic flow, is well known. Mach number distribution on the lower wall has a shock wave ($\max M \sim 1.37-38$) and the lower part of the shock wave has "Zierep singularity". We have tested position, strength, sharpness of the shock wave, appearance of the singularity and compared our results with the numerical results of other authors. We have also tested suitable combination of LW and LF steps and the influence of mesh and a scheme. We also present results in the geometry of the channel similar 2D cascade geometry.

Boundary conditions for transonic flows in GAMM channel are:

a) W_∞ is given on upstream boundary
b) non-permeability, reflecting boundary conditions are considered on the walls
c) pressure p is given on downstream boundary, other values of W are found by extrapolation.

We have solved the system of Euler equations (1) in 2D by time dependent method for steady solution of transonic flows in GAMM channel with $M_\infty = 0.675$ using cell-centered scheme (10)-(13) on a quadrilateral mesh (see Fig. 4) and cell-vertex scheme (14)-(16) on a triangular mesh (see Fig. 5). Fig. 4 shows Mach number distribution along the lower and upper wall. Fig. 5 presents also Mach number isolines. Comparison to the other numerical results (see [6]) achieved by Mac Cormack TVD scheme shows very good agreement.

We also show numerical results in channel changed by two bumps (stronger at lower wall, not so strong at upper wall) in Fig. 6.

Fig. 7 shows numerical result of 3D flow in a 3D channel with 2D GAMM channel geometry fixed in 2 directions and bump changing from 16% for $z = 0$ linearly to 8% for $z = z_{\max} = 1$. Mach number distribution in planes $z = z_k$ is shown.

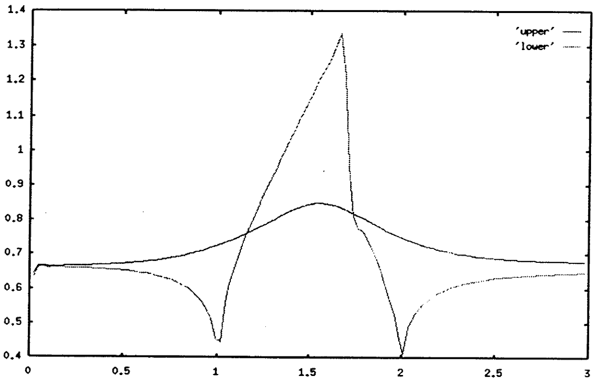

FIGURE 4. Distribution of Mach number for GAMM channel with $M_\infty = 0.675$ along upper and lower wall computed by cell-centered scheme (10)-(13) using quadrilateral cells.

Presented computations have been done on the grid of 180×30 cells in 2D and $180 \times 30 \times 12$ cells in 3D by the composite LWLFN scheme with N between 25 and 35.

4. Conclusion

New composite schemes for solving the system of Euler equations in 2D and 3D geometry has been presented. The cell-vertex and cell-centered forms of the LF and LW schemes have been developed by the finite volume method on triangular and quadrilateral 2D mesh. The cell-vertex form has been extended to 3D mesh. The composite scheme then combines several LW steps with one smoothing LF step. Numerical results show that both presented schemes are in the case of transonic flow computation reliable giving very good results. The schemes seems to be promising also for other cases of computations.

Acknowledgement

This work was partly sponsored by grants No. 101/98/K001, 201/99/0267, 201/00/0586 of GAČR and Research Plan MSM 98/210000010.

References

[1] R. Liska, B. Wendroff: *Composite Schemes for Conservation Laws*, SIAM J. Numer. Anal., 35(6):2250-2271, 1998.

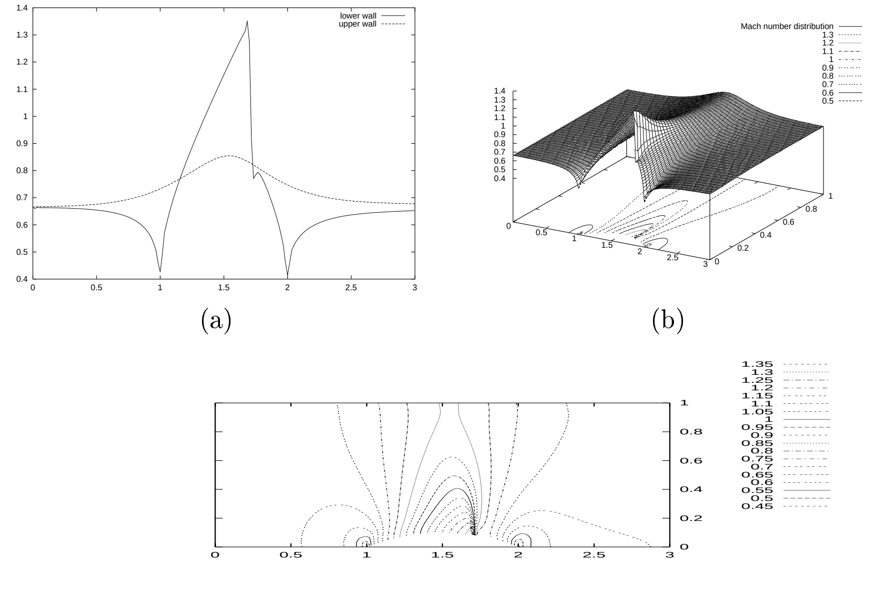

(a) (b) (c)

FIGURE 5. Distribution of Mach number M along upper and lower walls (a), surface of $M = M(x, y)$ in the GAMM channel (b) and isolines of Mach number (c). Results were computed by cell-vertex scheme (14)-(16) using triangular grid.

[2] R. Liska, B. Wendroff: *Two-dimensional Shallow Water Equations by Composite Schemes*, Int. J. Numer. Meth. Fluids, 30:461-479, 1999.

[3] M. Shashkov, B. Wendroff: *A Composite Scheme for Gas Dynamics in Lagrangian Coordinates*, J. Comp. Phys., 150:502-517, 1999.

[4] R. Liska, B. Wendroff: *Composite Centered Schemes for Multidimensional Conservation Laws*, In M. Fey and R. Jeltsch, editors, Hyperbolic Problems: Theory, Numerics, Applications, Seventh International Conference in Zürich, February 1998, Vol. II, pages 661-670, Basel, 1999. Birkhäuser, ISNM Vol. 130.

[5] P. Angot, J. Fürst, K. Kozel: *TVD and ENO Schemes for Multidimensional Steady and Unsteady Flows - A Comparative Analysis*, In "Finite Volumes for Complex Applications - Problems and Perspectives“, pp. 283-290, 1996 Rouen, Hermes-Paris, ISBN 2-86601-556-8.

[6] M. Feistauer, P. Knobloch: *Operator Splitting Method for Compressible Euler and Navier-Stokes Equations*, Proceeding of Workshop on Numerical Methods for the Navier-Stokes Equations, Notes on Numerical Fluid Mechanics, Vieweg, 1994.

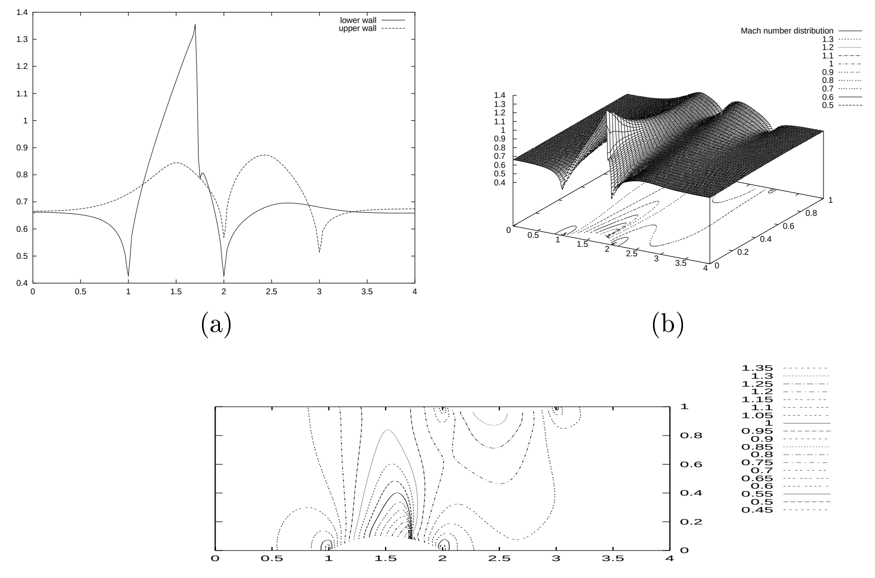

(a) (b)

(c)

FIGURE 6. Distribution of Mach number along upper and lower walls (a), surface of $M = M(x, y)$ in the GAMM channel (b) with two bumps (geometry of cascade) and isolines of Mach number (c). Results were computed by cell-vertex scheme (14) -(16) using triangular grid.

[7] J. Fořt, J. Fürst, J. Halama, K. Kozel: *Numerical Solution of 2D and 3D Transonic Flows Through a Cascade*, Proc. of ISAIF, Vol. I, pp. 231-240, TU Dresden, ISBN 3-86005-209-8.

Czech Technical University in Prague
Faculty of Mechanical Engineering
Karlovo nám. 13, 121 35 Prague 2, Czech Republic
E-mail address: `kozelk@fsik.cvut.cz`

Czech Technical University in Prague
Faculty of Nuclear Science and Physical Engineering
Břehová 7, 115 19 Prague 1, Czech Republic
E-mail address: `janda@km1.fjfi.cvut.cz, liska@siduri.fjfi.cvut.cz`

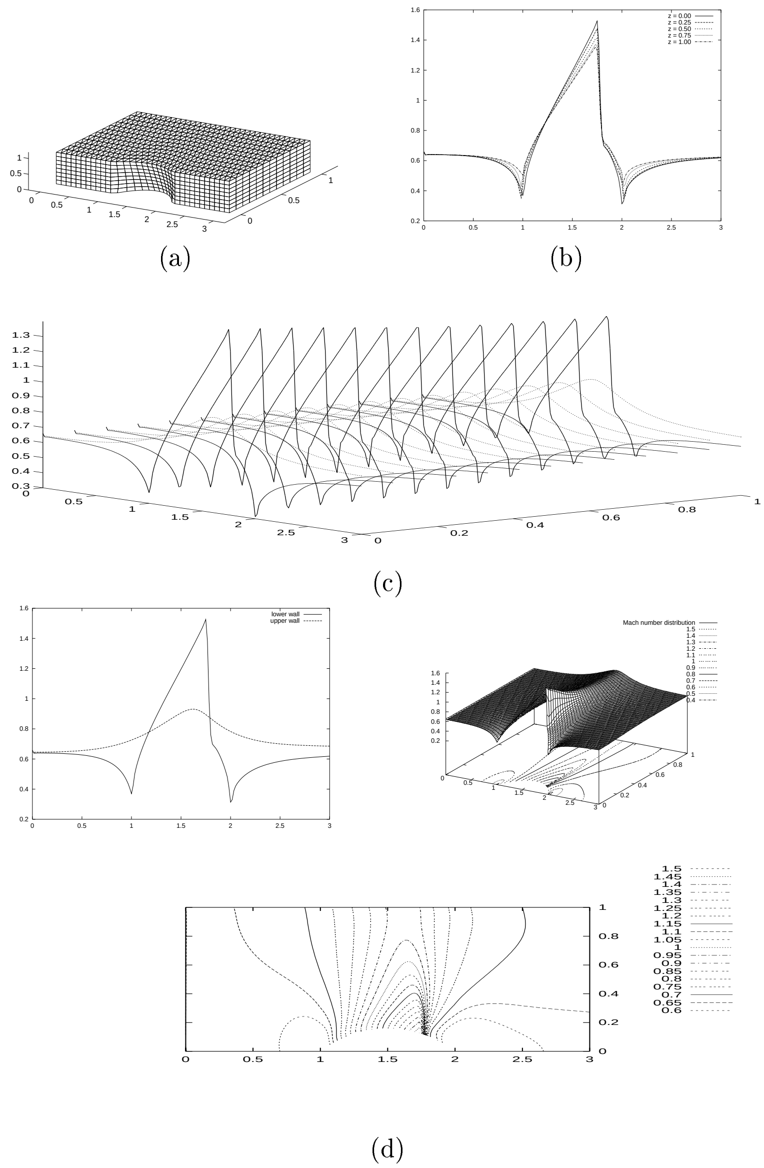

FIGURE 7. 3D results of flows in extended GAMM channel with bump changing thickness ratio in the third direction: (a) basic finite volume grid; (b) Mach number M distribution on lower surface, (c) M distribution along upper and lower surface for $z = z_k$, $k = 1 \ldots 12$, $z \in [0, 1]$; (d) results in the form of distribution of $M = M(x, y)$ and isolines of M for plane $z = 0$.